01 Jan 2023

Chemical Classification By Monitoring Liquid Evaporation Using Extrinsic Fabry-Perot Interferometer With Microwave Photonics

Abhishek Prakash Hungund

Bohong Zhang

Anand Nambisan

Wassana Naku

et. al. For a complete list of authors, see https://scholarsmine.mst.edu/ele_comeng_facwork/4855

Recommended Citation

A. P. Hungund et al., "Chemical Classification By Monitoring Liquid Evaporation Using Extrinsic Fabry-Perot Interferometer With Microwave Photonics," *Journal of Lightwave Technology*, Institute of Electrical and Electronics Engineers; Optica, Jan 2023.
The definitive version is available at https://doi.org/10.1109/JLT.2023.3273576

Chemical Classification by Monitoring Liquid Evaporation Using Extrinsic Fabry-Perot Interferometer with Microwave Photonics

Abhishek Prakash Hungund, Bohong Zhang, Anand Nambisan, Wassana Naku, Rex E. Gerald II and Jie Huang*

***Abstract*—Identification of liquids is essential in chemical analysis, safety, environmental protection, quality control, and research. A novel liquid identification system based on Microwave Photonics (MWP) measured time transient evaporation signals is investigated. An extrinsic Fabry-Perot Interferometer (EFPI) based optical probe using single-mode fiber (SMF) is proposed to monitor evaporation of different liquids. The MWP system is used to measure the optical path changes during liquid evaporation due to its high sensitivity, selectivity, and Signal-to-Noise Ratio (SNR). The measured S21 continuous wave (CW) time Magnitude and Phase signals were processed to extract features such as histogram and Fast Fourier Transform (FFT) peaks. Using features extracted from droplet evaporation time transient events, machine learning classification accurately identified chemicals in each liquid with an accuracy rate of over 99%, employing three algorithms: Decision Trees, Support Vector Machine (SVM), and K-nearest neighbors (KNN). The classification results demonstrate accurate liquid identification based on evaporation measurements by the MWP system.**

***Index Terms*— Single-Mode Fiber (SMF), extrinsic Fabry-Perot interferometer (EFPI), microwave photonics (MWP), Mach-Zehnder interferometer (MZI), decision tree, support vector machine (SVM), K-nearest neighbors (KNN).**

I. Introduction

Evaporation is the transition of the liquid phase to the gaseous phase under sufficient temperature conditions [1-4]. Study of evaporation process has a huge impact in chemistry, medicine, agriculture, biology, engineering, and several other applications [5-10]. The evaporation rates of chemicals or liquids vary depending on several factors external and internal such as vapor pressure [11], external temperature, humidity of the environment, concentration, and surface area of exposure [12]. Liquids with lower vapor pressure evaporate much faster due to their weak inter-molecular forces between the chemical's molecules as compared to liquids with high vapor pressure [13]. The temperature of the environment in which dip test is conducted forms an important factor impacting evaporation [14]. For having a typical temperature reference, the entire experiment and measurement was conducted at room temperature of 25ºC. Humidity is defined as the concentration of liquid vapor present in the air. Absolute humidity can be defined as the ratio of the mass of liquid vapor to the volume of air-liquid vapor mixture at room temperature. If the humidity is higher, the liquid evaporates much slower as there is an establishment of chemical equilibrium [15]. The concentration and surface area exposed to air also have a certain degree of influence on the evaporation rate of liquid. With an equal surface area of exposure, dilute liquids evaporate slower as smaller number of the liquid molecules are exposed to air [16]. The study of evaporation phenomena has been applied to several studies [17,18] which involve formation of sessile, pendant droplet and other standard micro-droplets. Different sensors based on mass and MEMS [19,20] are used to monitor the evaporation. They usually come with few drawbacks such as issues in measurement accuracy, power requirement, lack of compactness of sensor packaging and lack of immunity to electromagnetic interference (EMI). In recent times, dip tests are being employed to monitor evaporation and other chemical phenomena in liquids [21].

Dip tests have been vastly used as a standard probing mechanism in several chemical sensing applications [21-23]. The use of such test methodology for optical probing of liquid chemicals to measure the evaporation has recently been studied [24-26]. Dip tests performed on liquids usually involve immersing the probe into the liquid medium so that the probe breaks surface barrier of gas-liquid interface and rapidly pulled out [24,25]. This results in the formation of a droplet at the end face of the probing sensor. Several studies can be made from such droplets pertaining to evaporation, geometry, and manifestation, which are affected by the evaporation properties described earlier [25,26].

Fiber-optic sensing has several advantages: high sensitivity, no electromagnetic interference, compact, lightweight, robust, flexible, and capable of multiplexed and distributed sensing [23-31]. For example, Femto-second laser etched Fiber Bragg Grating (FBG) sensors and Distributed Sensing Systems (DSS) are being deployed in industry for high temperature sensing

J.H. is grateful for support from the Roy A. Wilkens Professorship Endowment. The views and opinions of authors expressed herein do not necessarily state or reflect those of the United States Government or any agency thereof. (Corresponding author: Jie Huang, jieh@mst.edu).

Abhishek Prakash Hungund, Bohong Zhang, Anand K. Nambisan, Wassana Naku, Rex E. Gerald II, and Jie Huang are with the Department of Electrical and Computer Engineering, Missouri University of Science and Technology, Rolla, MO 65409 USA (e-mail: jieh@mst.edu).

applications along with Rayleigh scattering-based distributed sensing system [28]. Another example points to using an optical accelerometer sensor for measuring low frequency vibrations in environment with high electromagnetic interference [31]. In addition to these features, optical fiber is also sensitive to the optical path difference making it a suitable candidate for sensing subtle variations in the cavity length [32] and/or external medium's refractive index (RI) [33-35]. Several EFPI sensors use fiber optics to detect RI changes, measuring gas concentration, strain, temperature, and pressure [36-39]. The fiber optic EFPI sensing systems have very high sensitivity to optical path changes as referenced in [40]. Due to these advantages, the single-mode fiber optic cable is configured as an EFPI for this research.

Using a standard optical interrogator having swept laser, the FSR (free spectral range) shift is monitored, which can be converted to the EFPI cavity length variation from the acquired interference spectrum. Some systems that use Optical Spectrum Analyzer (OSA), which can also acquire the EFPI interference spectrum [24], from which the FSR can be obtained and processed to compute the cavity length [41]. It is simple but expensive and slow regarding high-resolution measurements. To boost the speed, an edge filter can be configured as an optical interrogator [42]. Nevertheless, it results in poor accuracy due to source power drift and instability of the edge filter. Another way is to use a high-speed scanning optical filter, to achieve high-speed and high-resolution in measurement [43]. However, in such cases, the scanning range of wavelength is limited, and the resolution may drop if a wide wavelength band is needed. Microwave photonics interrogation is used to overcome these issues. MWP sensing mechanism involves the translation of optical domain wavelength shift to microwave domain Radio Frequency (RF) shift. They not only have high speed and high resolution in measurement [44] but also have improved performance in terms of selectivity, sensitivity, and SNR [45,46]. They are also stable and capable of multiplexed and distributed sensing features [47]. A DFB laser light of 1550nm wavelength is modulated with a 12 GHz RF signal from VNA is used as the source. The reflection from the optical probe is converted to an RF signal from Photodetector and fed back to the VNA. The modulation in light source with RF signal provides the high sensitivity in measurement which very suitable for this research purpose [48] as it can measure the optical path difference in RF domain as S-parameters.

Using Microwave Photonics, the S-parameters can be measured, particularly S21 (transmission coefficient) signal for this case, which can be used to describe the performance of the SMF optical probe in the frequency domain. Here, the S21 signal is the power transferred from port-1 to port-2 of the VNA through the optical path. Several different systems utilize the acquired S21 signal either in the time or frequency domain for sensing and signal integrity applications [49-52]. They are also measured with a reflection coefficient (S11) while studying the antenna performance [53]. The DBF laser's 1550nm light modulated with a 12 GHz RF signal, passes through the SMF probe and its reflection from the EFPI cavity is converted to RF signal and received at port-2 of the VNA through a high-grade coaxial cable. With 12 GHz frequency, a unique S21 recovery trend is observed towards the end of evaporation measurement for each liquid. Since single RF frequency of 12 GHz is used to modulate the light source from the DFB laser, the mode of sweep is set to CW time which measures S21 phase and magnitude signals in continuous time. The time transient S21 phase and magnitude signals show length and intensity variations in continuous time. These signals can be used to identify the liquids and study the evaporative nature of the liquid itself with respect to time.

Nowadays, classifying, identifying, and detecting chemicals have become necessary medicine/pharmacy, material science, environmental engineering and automotive [54-58]. Machine learning and deep learning methods [24] are being extensively used in such applications for classification and detection [59]. Deep learning techniques such as artificial neural networks (ANN) are used to find hidden information within signals for classification [60]. The S21 signals in our evaporation measurement have prominent and outstanding information for the classifier to learn. Hence, the traditional machine learning classifiers were applied such as Decision Trees, SVM and KNN, as they are easy to train and optimize when compared to deep learning methods. Data analytic methods such as these are also used in chemical health and safety research for classification [61]. Features such as Histogram and FFT peaks are extracted to train our classifiers. Histogram features from data are used in feature engineering and in understanding the phase behavior of chemical mixtures [62,63]. FFT features are used in several object detection applications [64], disease prognosis enhancement [65]. Hence, histogram and FFT peaks from the acquired data are used to train Decision Tree, SVM, and KNN classifiers.

In this article, to overcome issues with respect to measurement accuracy, packaging, and EMI, an SMF based optical probe is suggested. A short SMF cable with cleaved end face is mounted on linear stage. The evaporation phenomenon of the droplet formed at the optic fiber tip is measured and processed to identify the liquid chemicals. Since many measurements for multiple test liquids are needed, 6 liquids with low vapor pressure in addition to water are chosen, to get quick successive measurements. Hence, a total of 7 different types of liquid chemicals are tested, on which, multiple sets of controlled dip tests are carried out. In summary, a novel Microwave Photonics CW time measurement over the standard optical interrogation methods for monitoring evaporation phenomena of liquids is proposed. S21 CW time magnitude and phase signals are acquired from which histogram and FFT features are extracted, and machine learning classifiers are trained to identify those liquids. The trained classifiers are validated on a separate hold-out dataset obtained by experimenting at different times. From the results it can be observed that classifiers perform quite well on identifying the liquids. And particularly, SVM stands out in its performance, by giving test accuracy greater than 99%. The other classifiers also perform well after their optimization and tuning.

II. MEASUREMENT AND SENSOR SETUP

A. *Experimental Setup*

The proposed system is constructed with a simple setup. Sensor is single-mode fiber with cleaved end face used as an optical probe for dip measurement. The optical probe is kept as short as possible (30cm) to obtain maximum sensitivity in S21 phase variations. The optical probe length can be reduced further to obtain even higher sensitivity but may have trade-off with SNR. It is mounted on a Newport FCL50 linear motor stage and the fiber is connected to a single-mode 2x1 optical coupler's sensing arm. One arm of the optical coupler is connected to the source, and the other arm is connected to a Keysight Lightwave Detector (Keysight N4377A-M40) with a bandwidth of up to 40 GHz. The complete experimental setup or block diagram is shown in Fig. 1b.

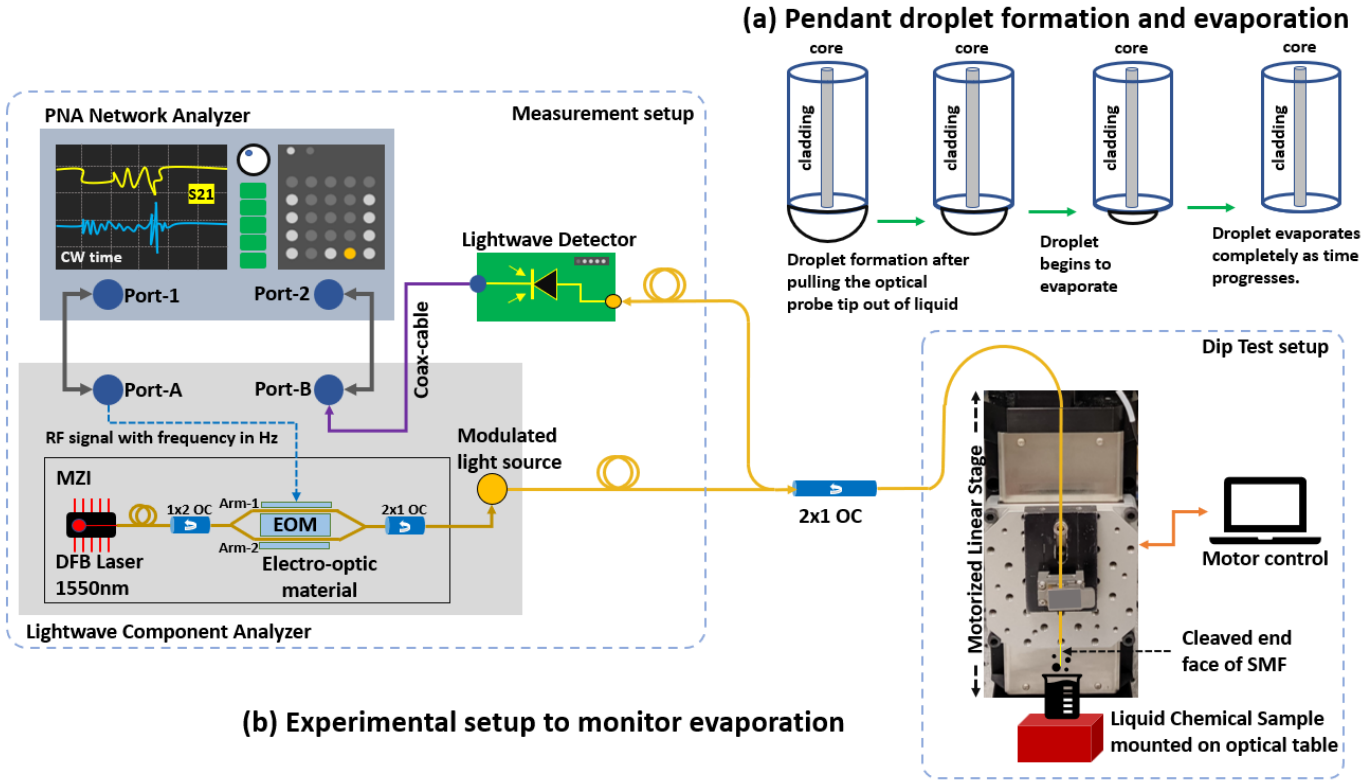

Fig. 1. (a) Pendant droplet formation and evaporation. When the optical probe is pulled out of the liquid, the droplet forms at the tip of the fiber and starts to evaporate with time. (b) Experimental Setup to study the evaporation of the pendant droplet EFPI of liquid sample. The port-1 of Performance Network Analyzer (PNA) is connected to Lightwave Component Analyzer's (LCA) Mach-Zehnder Interferometer (MZI) where the light from Distributed Feedback (DFB) laser is modulated by RF signal. The source port from LCA is connected to one arm of Optical Coupler (OC). The sensing arm of the OC is connected to a cleaved Single-Mode Fiber (SMF) which is the sensor. The other arm of OC is connected to a Lightwave Detector (LD). The LD is connected to the port-2 of PNA through a coaxial cable.

A high-grade coaxial cable from Lightwave Detector is connected to port-2 of the PNA Network Analyzer which is employed to measure the time domain S21 phase and magnitude signals in CW time sweep mode. The DFB laser light source of 1550nm with a power of 5 dBm is generated by Keysight Lightwave Component Analyzer N4375E. It is modulated with the RF signal of 12 GHz with a power of 5 dBm from port-1 of the Keysight PNA Network Analyzer N5222B having a bandwidth of 10 MHz to 26.5 GHz. The Keysight Lightwave Component Analyzer contains a Mach-Zehnder Interferometer (MZI) that has 2 different arms which have electro-optic material such as Lithium Niobate (LiNbO3) for electro-optic modulation (EOM). The light from DFB source is amplitude modulated and split into two arms of the MZI. In each arm of the MZI, the optical signals are subjected to phase modulation by the RF signal from port-1 of PNA. The modulated light from MZI is used for sensing. Microwave photonics are used here to perform AC measurement for recording the evaporation process shown in Fig. 1a. MWP provides additional phase information which cannot be obtained when using a traditional optical interrogator. The phase information acquired in realtime is a direct measure of the length variations due to evaporation. Standard optical interrogation is capable of only DC measurement and cannot provide the phase data. The phase data is responsible for providing the length information of the droplet.

The SMF optical probe is a 1550BHP - 0.13 NA (numerical aperture), operating wavelength range – 1460 nm to 1620 nm, 125 µm fiber diameter, with FT900Y tubing. One end of the probe has FC/APC connector connecting to the optical coupler. The operating wavelength of the coupler is also 1550 nm. The liquid sample was placed in a cylindrical glass beaker and mounted on an optical table. As shown in Fig. 1b, the fiber is mounted on a vertical linear motor stage. The stage moves the fiber probe in and out of the liquid surface boundary. The stage's movement is controlled by a system having Newport motor software installed. Since there is no direct way to control

the droplet size, the velocity of the motor is set to constant. The pull-out height varies depending on the liquid sample's range of humidity from the liquid surface. An approximate control over the droplet size formation at the tip of the sensor probe can be established by using the motor stage. The experimental setup involving the measurement equipment and dip test setup are placed on an optical table which aids in isolating the setup from localized vibrations and other disturbances.

B. *Measurement Principle*

After performing the dip test on a sample liquid, as described in the previous subsection, a pendant droplet forms at the cleaved end face of the SMF optical probe. The droplet results

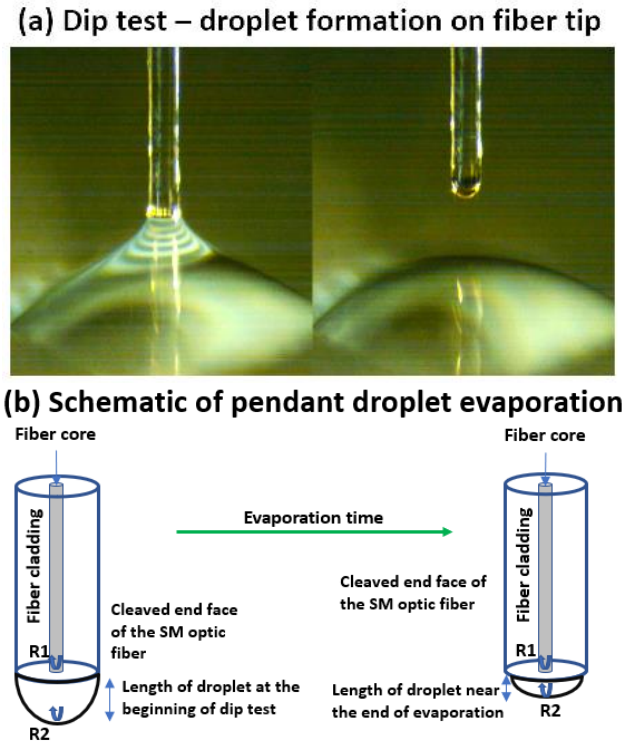

Fig. 2. Illustration of a pendant droplet evaporation phenomenon on the cleaved end face of the SMF probe for a liquid test sample. (a) Droplet formation on probe tip from the dip test (b) Schematic illustrating droplet formation and evaporation. R1 and R2 are the reflections from the first and second reflectors of the droplet EFPI. The reflector R2 moves closer to R1 as the liquid droplet evaporates.

in the formation of 2 interfaces; the fiber-liquid interface, and the liquid-air interface. Due to these interfaces/reflectors, the modulated light coursing through the probe undergoes two reflections that interfere to form a temporary EFPI whose cavity length gradually decreases with time due to evaporation as shown in Fig. 2b. The equation (1) provides the light intensity reflected from the proposed EFPI system.

$$I = I_1 + I_2 + 2\sqrt{I_1 I_2}\cos[\Delta\phi + \phi_0] \quad (1)$$

where, I_1 is the reflected intensity at the fiber-liquid interface and I_2 is the reflected intensity at the liquid-air interface, ϕ_0 is the initial phase difference, and $\Delta\phi$ is the relative phase change due to variation in cavity length, represented by the equation:

$$\Delta\phi = \frac{4\pi\Delta(nl)}{\lambda_m} \quad (2)$$

where, n is refractive index of the medium, l is the cavity length of EFPI and λ_m is the narrow wavelength band of modulated light. The variation in reflected light intensity is directly proportional to the droplet's cavity length variation. As the droplet evaporates, the cavity length decreases gradually. Due to shortening of the cavity length, time-varying light intensity generates photo-current with oscillating power. The power fluctuation results in oscillating S21 time series magnitude and phase. And as the droplet evaporates, there will be slow dynamic decrease in the total length, that gives us varying S21 time series phase data unique to each liquid. Time transient S21 phase and magnitude signals are recorded for each liquid sample. These signals are processed further for feature extraction which are used to train liquid identifying classifiers.

C. *Mach-Zehnder Modulator*

The Lightwave Component Analyzer (LCA) modulates the optical signal through the RF signal utilizing an MZI, as shown in Fig. 1b. While describing modulation, it becomes important to explain how the optical signal is modulated. An optical source's input electric field E_{in} is split into two arms of the MZI. In arm-1 of MZI, the optical signal undergoes phase modulation, which is different from phase modulation in arm-2 due to the bias voltages as shown in Fig. 3. For simplicity, the light interference from two arms is assumed to have equal amplitude [66]. After recombination, the total electric field is given by:

$$|E_{out}^2| = |E_1 + E_2|^2 \quad (3)$$

Equation (3) represents the optical power of modulated signal shown in Fig. 3. The modulated light passing through both the arms are given by:
Arm-1:

$$E_1(t, d_1) = P\sqrt{1 + Q\cos\left[\gamma\left(t + \frac{L+d_1}{c}\right)\right]} \cdot e^{\left[-j\omega\left(t+\frac{d_1}{c}\right)\right]} \quad (4)$$

Arm-2:

$$E_2(t, d_2) = P\sqrt{1 + Q\cos\left[\gamma\left(t + \frac{L+d_2}{c}\right)\right]} \cdot e^{\left[-j\omega\left(t+\frac{d_2}{c}\right)\right]} \quad (5)$$

where t is time, P is amplitude of optical carrier signal, Q is amplitude of RF signals, γ is frequency of RF signal, ω is optical signal frequency, c is speed of light in optical fiber. L is electrical length of RF path (coaxial cable), d_1 and d_2 are optical lengths of MZI arm. Substituting (4) and (5) in (3), one can obtain the power of modulated signal as:

$$|E_{out}^2| = 2P^2 + 2P^2 Q\cos\left[\gamma\frac{d_1-d_2}{2c}\right]\cos\left[\gamma\left(t + \frac{2L+d_1-d_2}{2c}\right)\right] + 2P^2\sqrt{\left(1 + P\cos\left[\gamma\left(t + \frac{L+d_1}{c}\right)\right]\right)\left(1 + P\cos\left[\gamma\left(t + \frac{L+d_2}{c}\right)\right]\right)} \cdot \int_{\omega_{min}}^{\omega_{max}} \cos\left(\omega\frac{d_1-d_2}{c}\right) d\omega \quad (6)$$

Equation (6) has 3 different parts which include DC, RF signal and optical signal fields. When the optical path difference becomes longer than the coherence length, integral part of the optical signal term approaches zero and the RF signal part removes the DC to provide magnitude and phase information making it AC measurement. The modulated optical signal used for sensing in this investigation is shown in Fig. 3. The total length, which includes the RF electrical length and the optical probe length, affects the phase measurement. The polarization of the source and the EOM should be parallel to increase the modulation efficiency.

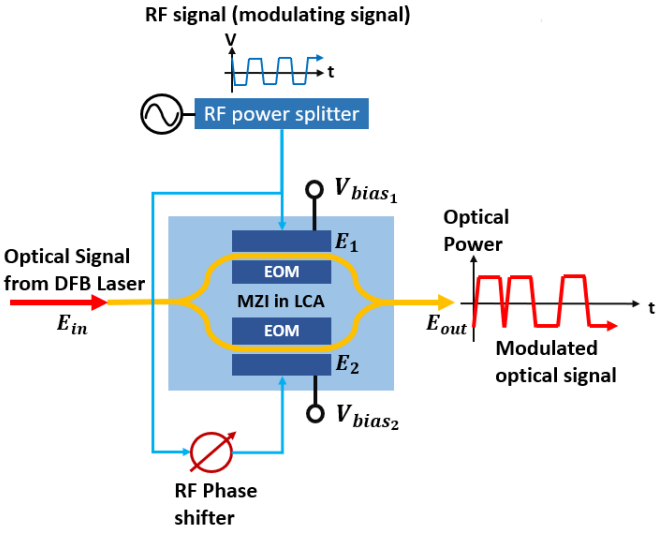

Fig. 3. Electro-optically modulated Signal. Shows optical signal from DBF laser getting modulated by the RF signal, which is generated from the Lightwave Component Analyzer, LCA. The modulated optical signal coming out of the EOM is used to perform AC measurement of the evaporation.

III. DATA ACQUISITION AND PROCESSING

Seven different liquid samples were used for testing the proposed system. For each liquid sample, 80 measurements were carried out to obtain S21 CW time magnitude and phase signals. The time series data obtained were from 0 to 38 seconds. Each signal has 20000 points from 0 to 38 seconds that covers the liquid sample's evaporation time. Measurements for all liquids are conducted at a room temperature of 25ºC. The S21 signals are affected by temperature and humidity, with higher temperatures potentially revealing additional features, while each chemical exhibits a consistent and unique recovery trend in the S21 signals. The network analyzer was set to sweep in CW time S21 mode with an RF frequency of 12 GHz, power of 10 dBm, 20000 points, and IFBW of 500 Hz. A low sweep rating (IFBW) was set to accommodate liquids with lower vapor pressure. A 1550 nm DFB laser source was modulated with a 12 GHz RF signal frequency for the light source. The IFBW (Intermediate Frequency Bandwidth) of the average bandwidth can be set higher or lower per the target liquid's evaporation time. The dip tests on each liquid were conducted using a linear motor stage to test the system's repeatability and reliability. Dip tests are carried out by the optical probe mounted on the linear motor stage, which enables the control of droplet size on the probe tip and minimizes the shaking during dipping process.

It was observed that the implemented setup was highly selective while measuring the S21 signals for each chemical sample. 80 dip tests were performed to obtain S21 CW time magnitude and phase signals. Features were extracted to train the classifiers based on the collected signals. First the S21 CW time magnitude signal was converted to a linear scale. Following that, mean retention was used to normalize both S21 CW time magnitude and phase signals. Since the captured signals had a good SNR, no filtering was used. The high frequency components in the signals serve as features for training the classifiers. As part of data pre-processing, the requirement for classification using machine learning is the class label encoding of the chemical samples which was done as the per TABLE I shown below:

TABLE I
CLASS LABEL ENCODING FOR CHEMICALS

CHEMICAL	CLASS LABEL
Acetone	0
Ethanol	1
Heptane	2
Hexane	3
Methanol	4
Water	5
Iso-propyl Alcohol (2-propanol)	6

For training purpose, 7 chemicals are represented by their respective class labels (numerical values) in this research.

A. *Feature Extraction and Machine Learning*

For each measurement of a liquid sample, histogram and FFT features are extracted. The advantage of using histogram features is that it provides information about the value having the highest weight in the signal. And FFT features like the peaks give us information about different frequency components in the time series signal. Hence, a histogram of 100 bins with bin limits of [0, 0.94], for each S21 CW time magnitude and phase signal of a liquid was obtained. In case of phase, the bin limits translate to a span of [-360º, 316º], with the total phase span being [-360º, 360º]. In addition, 75 peaks from the FFT of the S21 CW time magnitude signal and 100 peaks from the FFT of the S21 CW time phase signal were extracted, which are the minimum number of predictors required to obtain the desired accuracy. These features are eventually concatenated to create a vector of 375 predictors. Feature predictor vector is used to train classifiers with the liquid sample's encoded class label as target. The phase fluctuations that occur during the evaporation process are measured using microwave-photonics in real-time. Compared to using features only from the S21 CW time magnitude signal, the derived features better identify the liquids. These findings indicate that the S21 CW time phase signal captures droplet shrinkage-related real-time length fluctuations. Furthermore, by minimizing fiber length, highly sensitive measurements were realized. A machine learning classification scheme is proposed

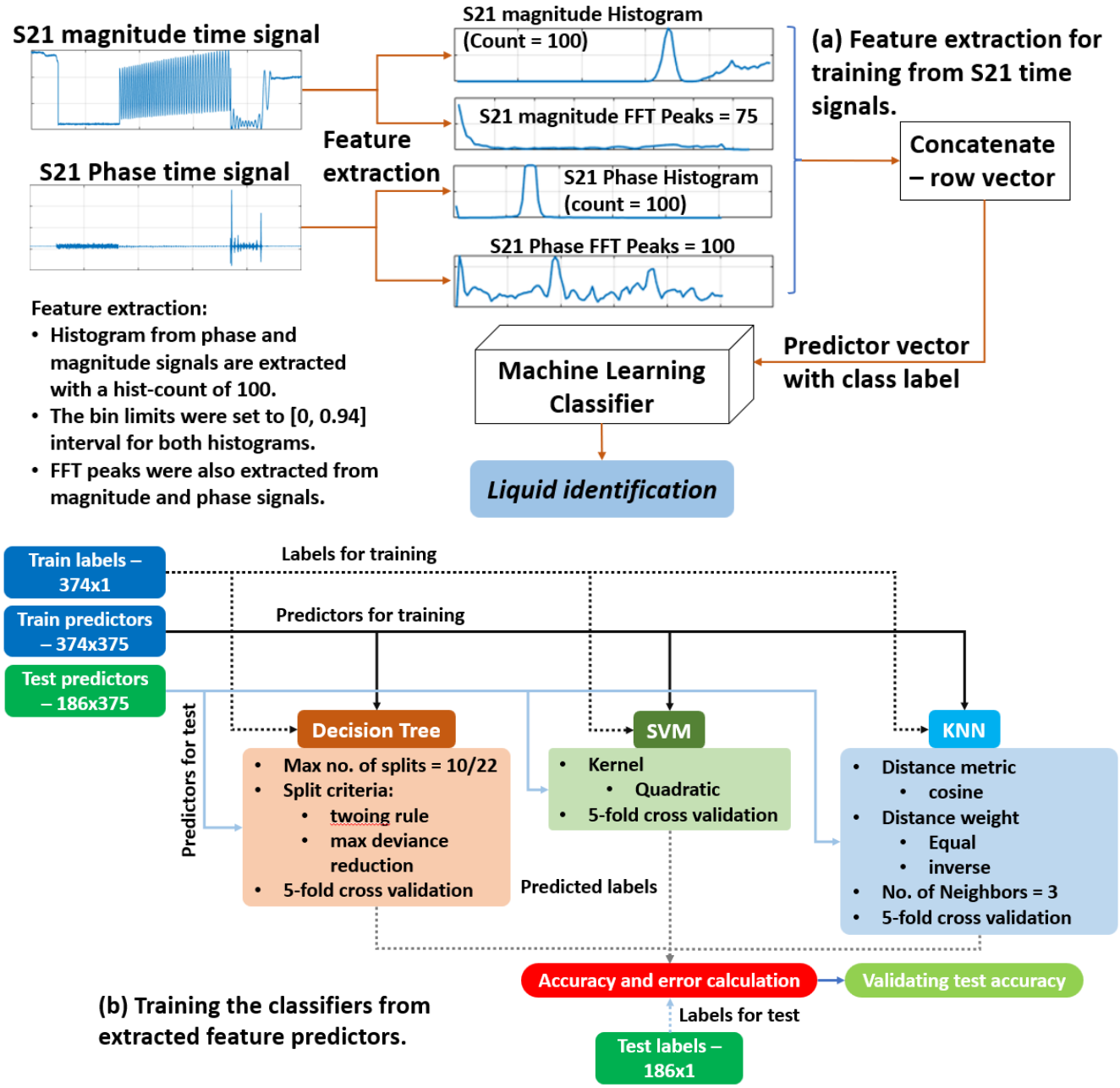

Fig. 4. Machine learning classification training process. (a) Illustration of feature extraction from the S21 CW time magnitude and phase signals measured by the PNA and process of classification using machine learning. (b) Process of training the classifiers from extracted predictors/features with matrix and vector sizes and identifying liquids from each classifier. The classifier blocks also show tuned parameters for classifier optimization.

to identify the liquids rather than meticulously calculating the evaporation rate from the acquired S21 CW time signal. The S21 CW time magnitude and phase signals have outstanding features regarding the evaporation process unique to each liquid sample being tested. Several applications propose deep neural network techniques such as convolutional neural network (CNN), artificial neural network (ANN) and recurrent neural networks (RNN) to address classification challenges. Those methods are useful and applicable when signals have features hidden in the signals. However, complicated pre-processing, training time and computational cost are drawbacks from the previous methods. The suggested microwave photonics measuring technique enables the observable signal features that the traditional machine learning classifiers like Decision Trees, SVM, and KNN, can learn. These classifiers can be learned effectively and quickly from extracted feature predictors like histograms and FFT peaks. The training scheme is shown in Fig. 4a. The features are used for training 3 different classifiers such as Decision Tree, SVM and KNN out of which, SVM gives the best performance. Decision Tree parameters, max no. of splits = 22, split criteria = max deviance reduction, training time = 1.1416 seconds, and total misclassification cost = 15. SVM parameters, kernel function = Quadratic, training time = 1.6691 seconds, kernel scale = 1, and total misclassification cost = 1. KNN parameters, no. of neighbors = 3, training time = 0.82836 seconds, distance metric = cosine, distance weight = equal, and total misclassification cost = 6. 5-fold cross validation was done to validate the classifier performance. The

binary SVM classified the input data by finding the optimal hyperplane having the largest margin between any 2 classes. The SVM was extended for multi-class classification by combining several binary SVM models utilizing ensemble methods like error correcting output codes (ECOCs) [67].

B. Accuracy and Loss metrics

After the classifier was trained, a new set of measurements was taken. These new measurements were processed to extract features and used as predictors on the classifiers, identifying the liquids with very high accuracy. The prominent part to note here is that the classifier was tested on a dataset that was not seen in the training dataset. These classifiers were trained as per the flow shown in Fig. 4b. The accuracy of a classifier is defined as the ratio between number of correct predictions to total number of predictions and is expressed by equation (7):

$$Accuracy = \frac{Number\ of\ correct\ predictions}{Total\ number\ of\ predictions} \tag{7}$$

Elaborating equation (7), the accuracy can be derived as:

$$Accuracy = \frac{\sum_{j=1}^{N} F\{y_j == \hat{y}_j\}}{N} \tag{8}$$

where, N is the number of predictions, y_j is an observation of actual target label and $\hat{y}_j$ is an observation of predicted target label. F is the indicator function indicating the number of predictions matching the corresponding actual targets. The misclassification cost $\mathrm{C_m}$ is essentially weights applied to specific outcomes, which is estimated as:

$$C_m = \sum_{j=1}^{N} w_j c_{y_j,\hat{y}_j} \tag{9}$$

where, w_j is the weight value associated with the observation j, $\hat{y}_j$ is the predicted class label, y_j is the actual class label and $c_{y_j\hat{y}_j}$ is the user specified cost for classifying an observation. Correspondingly, Hinge loss H_L is calculated as:

$$H_L = \sum_{j=1}^{N} w_j\, max\{0, 1 - m_j\} \tag{10}$$

where, m_j is the classification score for classifying the observation j into the class corresponding to y_j which is expressed as:

$$m_j = y_j f(X_j) \tag{11}$$

where, $f(X_j)$ is the positive/correct-class classification score for observation j of the predictor feature X.

MATLAB's classification learner toolbox was used to train the classifiers. The training time is less than 2 seconds on average for the classifiers being trained here. To accelerate the training time, MATLAB's Parallel Computing toolbox was used, optimizable models were trained initially for model parameter tuning with different combinations of parameters. The use of GPU is unnecessary here as there is no training involving deep neural networks. Moreover, the dataset used for training here is considerably smaller. Unlike deep learning, traditional classifiers such as SVM and KNN allow for better control over the intermediate training steps and are comparatively easier to optimize. However, the features of interest in the training data should not be hidden in the signals when training traditional machine learning classifiers.

IV. EXPERIMENTAL RESULTS AND DISCUSSION

The primary goal of this article is to develop a simple fiber optic probe that can detect and classify liquids using a traditional machine learning classifier. Training Decision Trees, SVM, and KNN classifiers enables for a data-analytical approach. Seven liquid test samples (acetone, ethanol, heptane, hexane, methanol, water, and iso-propyl alcohol or 2-propanol) with important physical properties are shown in TABLE II. The vapor pressure influences the evaporation rate of the liquids as generally demonstrated by its inverse relationship to droplet evaporation time span. But surface tension and other properties of the liquid complicates this relationship. The molar mass also has a certain degree of effect, i.e., the larger the molecule, the lower the evaporation rate. Also, the higher the boiling point, the lower is the evaporation of the liquid. molecular density has an indirect control over evaporation rate, where liquids with higher density experience greater intermolecular forces, thereby resulting in slower evaporation. The refractive index (RI) can become an indication of the above chemical properties of each liquid making it a suitable parameter to measure. A unique S21 CW time magnitude signal oscillation is observed due to the varying optical path during liquid evaporation. This is due to the droplet being perceived as a varying electrical resonator by the MWP system.

A total of 560 dip tests were performed on 7 liquids, i.e., 80 measurements for each liquid as shown in TABLE II. In Fig. 5 the S21 CW time magnitude and phase signals are presented from each liquid's droplet evaporation phenomenon. From these, the unique information pertaining to evaporation of each liquid can be observed. It was possible to obtain such evident measurement due to the highly sensitive nature of the EFPI. When combined with microwave photonics, it was possible to obtain high selectivity in the sensing mechanism. There is a clear difference in the signals of each liquid shown in Fig. 5a. However, it becomes difficult to classify by visual inspection alone for certain liquids. For example, the S21 signals of heptane and hexane are very similar, making it challenging to classify. Hence, machine learning classification is used, which can provide a data analytical approach. The trained classifiers can recognize the difference between cosmetic anomalies and actual differences relevant to each S21 CW time signal.

The measured S21 CW time signals of the evaporation phenomena provide outstanding information regarding refractive index, evaporation rates, length variations and recovery trend which is a positive consequence of the EFPI's highly sensitive nature. Calculating the evaporation rate directly using the S21 CW time signals to identify the liquid

TABLE II
PHYSICAL PARAMETERS OF THE LIQUIDS IN THIS STUDY

CHEMICAL	FORMULA	MOLAR MASS (g/mol)	BOILING POINT (ºC)	SURFACE TENSION at 25 ºC (mN/m)	VAPOR PRESSURE at 25 ºC (mmHg)	EVAPORATION TIME SPAN (Seconds)	DENSITY (Kg/m^3)	REFRACTIVE INDEX (RI)
Water	H_2O	18.02	100	72	23.686	12.45	998.2	1.333
2-propanol	C_3H_8O	60.1	82.5	22	43.646	9.97	786	1.377
Heptane	C_7H_{16}	100.21	98.44	20.4	45.59	0.91	684	1.387
Ethanol	C_2H_6O	46.07	78.38	22.27	58.753	1.85	789	1.361
Methanol	CH_3OH	32.04	64.72	22.50	126.87	11.27	792	1.329
Hexane	C_6H_{14}	86.18	69	18.4	151.19	0.86	655	1.375
Acetone	C_3H_6O	58.08	56	26.2	229.46	2.09	784	1.359

Chemical formula of liquids is presented with its corresponding Molar Mass, Boiling Point, Surface Tension, Vapor Pressure, Evaporation Time Span, Density and RI.

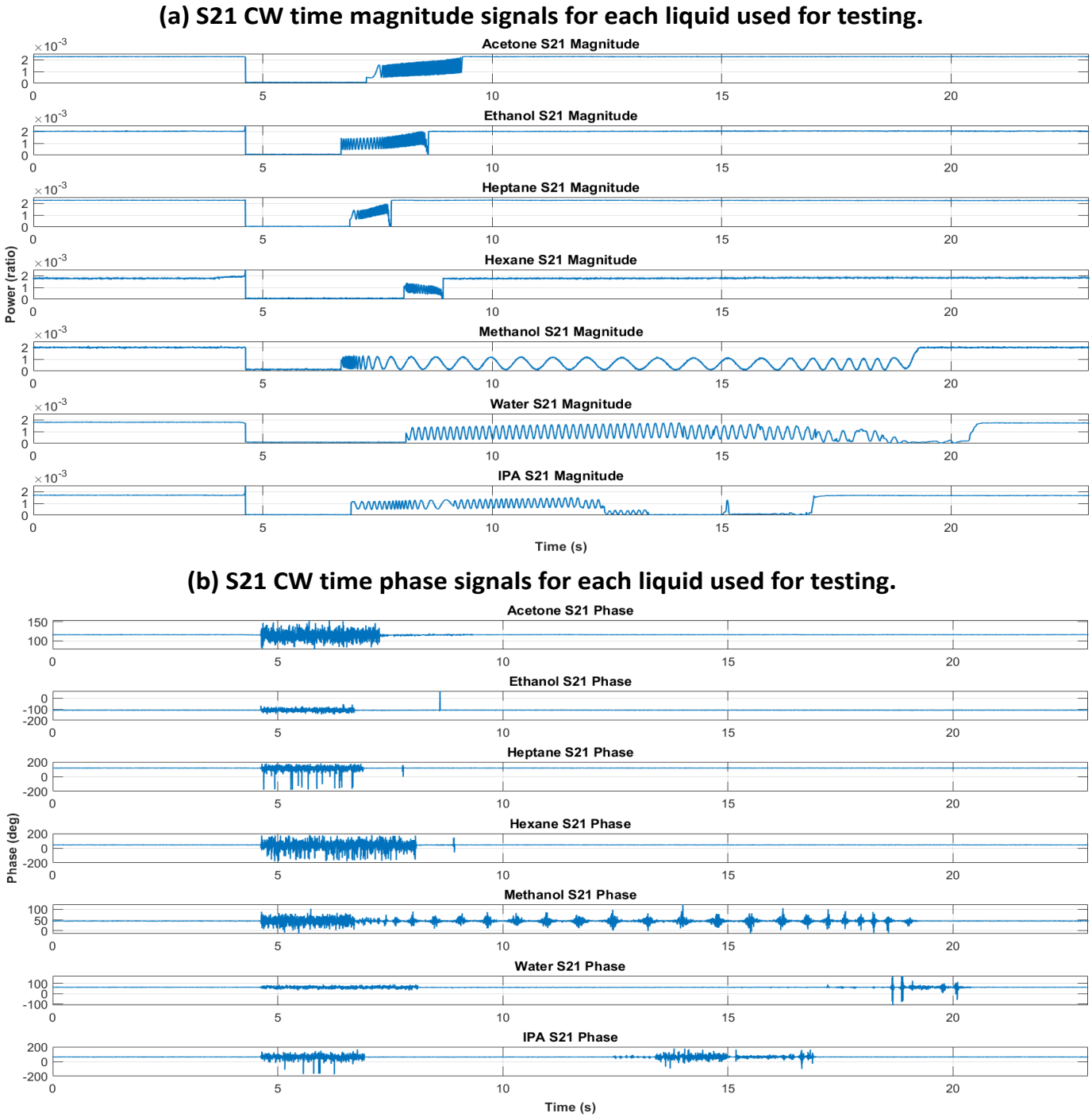

Fig. 5. S21 CW time magnitude and phase signals of 7 liquids. (a) S21 time transient magnitude signals measuring evaporation of each liquid and (b) S21 time transient phase signals depicting length variation during evaporation of each liquid. The plots correlate evaporation phenomena with droplet size variation of all the liquids.

would result in the loss of some important features and could give incorrect result. Thus, traditional machine learning is used to learn features in the signals for classification. The results show that trained classifiers work quite efficiently in classifying the liquids based on the evaporation data measured by the SMF probe with MWP. The SVM, KNN and Decision Tree classifiers require a reasonable amount of data for effective performance. The large volume of data can be obtained only through repeated experimentation which can get tedious. Thus, measuring repeatability is of primary importance here.

According to the results in Fig. 5a and Fig. 5b, few conclusions can be made. As soon as the optical probe is dipped into the liquid, the power level drops in S21 CW time magnitude signal and the phase variations increases in S21 CW time phase signal. The drop in power level and change in phase variations are unique to each liquid due to the effective refractive index of each liquid. The higher the refractive index of the liquid, lower is the SNR and higher is the variations of the phase. The variations in S21 CW time phase signals when the optical probe is immersed in the liquid is dependent on the loss of power within the liquid. The more the power level drops in magnitude signal, higher is the phase variations measured by the phase signal. The study of these unique phase responses can aid in the detecting of binary liquid mixtures which shall be studied in future. The RI is a clear indication of change in the medium from air to corresponding liquid. In this experiment, the immersion depth and dipping speed are maintained constant to get a consistent droplet size, as it can influence the evaporation rate.

When the optical probe is pulled out of the liquid medium, a droplet forms at the probe's tip. This droplet is perceived as an electrical resonator by the MWP system. The droplet, while evaporating exhibits resonant behavior with a very high reactive peak at its resonant frequency. During evaporation of the liquid droplet, the resonant frequency remains constant as the surface tension remains constant throughout the process [69]. But it is important to note that the pure liquid molecules resonate at different frequencies according to their vibrational and rotational modes, which have quantum origins and can be identified by infrared spectroscopy [70]. As the droplet evaporates, oscillations in the S21 CW time magnitude signal can be observed with different periods for each liquid sample as shown in Fig. 5a. Simultaneously, the phase changes in S21 CW time phase signal pertaining to those oscillations in corresponding magnitude signal can be observed and are shown in Fig. 5b. Liquids such as ethanol, heptane and hexane have minor variations in the phase which can be attributed to their chemical properties shown in TABLE II. Zooming into the Y-axis region in Fig. 5b, it is possible to see the periodic changes in phase for each liquid. Towards the end, when the droplet has almost evaporated, there are some quantum fluctuations in S21 CW time magnitude and phase signals, which make up for the unique recovery trend of each liquid. Due to the absence of a definite second reflector, clear interference does not occur which is responsible for unique recovery trend. Thus, different S21 variations for different liquids can be observed with this setup. However, there are subtle similarities for example, between heptane and hexane which is attributed to the presence or absence of certain hydrocarbon groups in these chemicals. Finally, the magnitude and phase reference levels recover after the droplet completely evaporates.

The chances of liquid or chemical residue on the optical probe are minimal for the liquids being tested in this research. Thus, there is no need for cleaning the optical probe after each

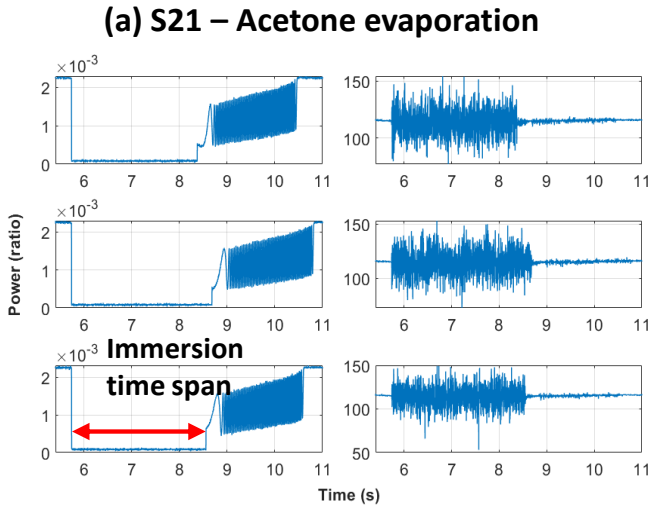

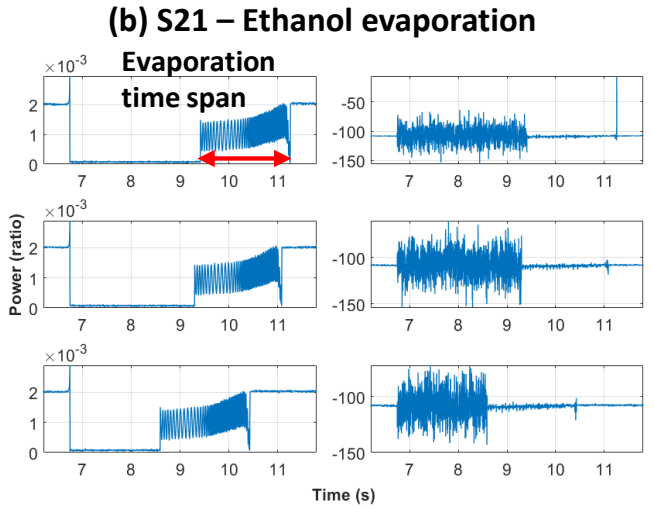

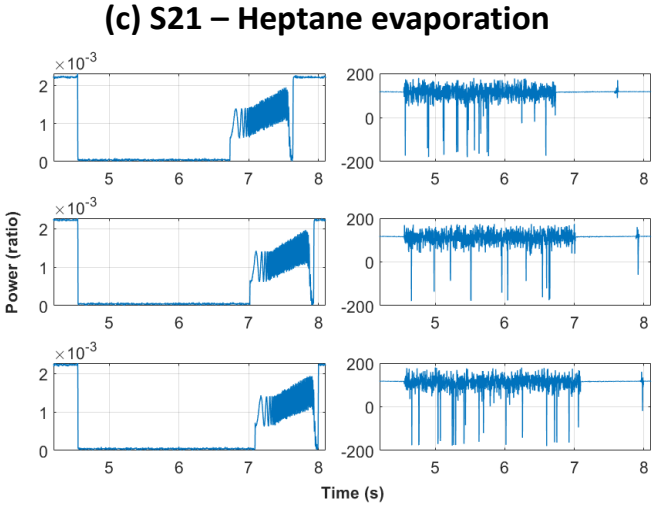

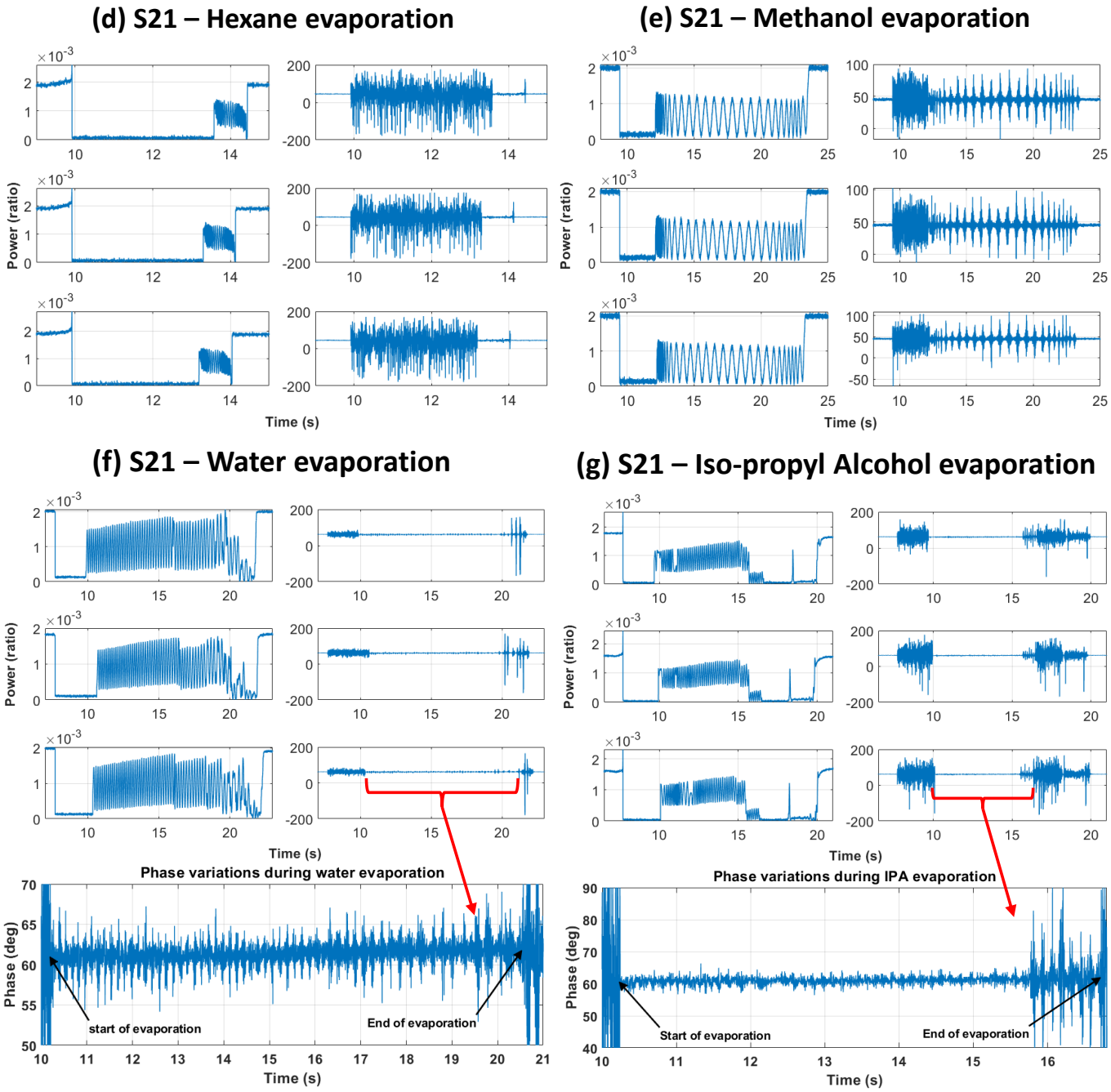

Fig. 6. S21 CW time magnitude and phase signals for all the pure liquids. These plots provide information about the average evaporation time of each liquid and their corresponding phase variations. For example, the data for droplet evaporation transient for methanol clearly demonstrates a unique signal pattern for the S21 CW time phase. These S21 phase patterns constitute additional and unique measured data that increase the accuracy of the classifiers. More typical examples would be water and iso-propyl alcohol which are presented in (f) and (g). The respective phase variations during droplet evaporation are explicitly shown. The features at beginning and the end of the droplet evaporation transient from phase data correlate well with the corresponding features from magnitude data thereby increasing the classifier's accuracy.

dip test. As shown in Fig. 6, the average evaporation time for each liquid sample was observed, which is approximated based on the total time span of oscillations in the S21 CW time magnitude signal. The time series magnitude and phase signals of each liquid evaporation are unique. For example, the magnitude signal of IPA in Fig. 6g, has a sharp spike towards the end i.e., during recovery after evaporation which can be studied to explain the quantum jump [68] phenomena of the iso-propyl alcohol during evaporation which will be explored in future experiments.

The time axis of signals in Fig. 6 is expanded so that the entire evaporation phenomenon is clearly visible for each liquid. The average evaporation time of each liquid is observed to be approximately repetitive. When the dip test is being performed, it is imperative that the probe is pulled high enough from the surface of the liquid such that the humidity at the liquid surface does not slow down the evaporation. All the signals acquired here have evaporation time according to their vapor

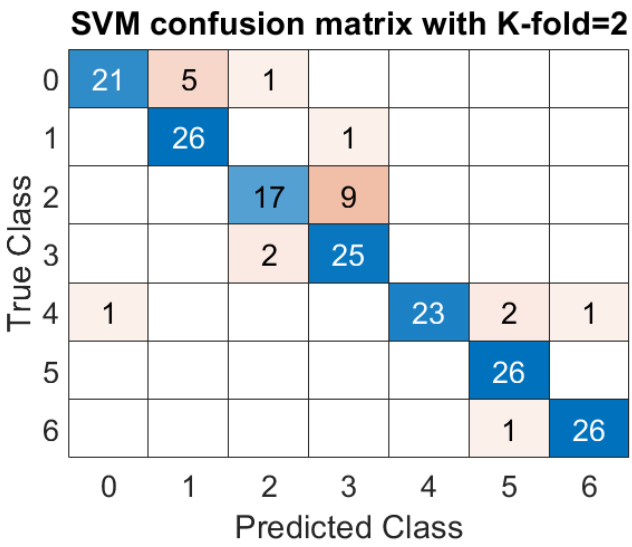

Fig. 7. Confusion matrix for SVM classifier trained with features extracted from only the S21 CW time magnitude signals of all 7 liquids. After training, the training accuracy was obtained as **87.76%** and the test accuracy was obtained as **84.45%**. Even with 3-fold, much improvement is not obtained.

of each dip tests are not synchronized due to the manual triggering of the linear motor stage. Nevertheless, repeated measurement shows that the classifiers can clearly identify liquids within a temperature tolerance of (25 ± 5) ºC, which allows for a wider temperature range for sensing.

Out of 80 measurements, 53 measurements were used for training. From magnitude signal, 100 histogram bins and 75 FFT peaks are extracted. From phase signal, 100 histogram bins and 100 FFT peaks are extracted. Initially, the features extracted from magnitude signal shown in Fig. 8 is concatenated to form vector of 1×175, for all 53 measurements of 7 liquids, giving a feature predictor matrix of 374×175. This matrix was split into training data of size 187×175 and test data of size 187×175. An SVM classifier was trained with 187×175 training data. This classifier was tested on the 187×175 test data whose results are presented in Fig. 7, along with the test and training accuracy metrics. From the confusion matrix, it can be observed that classifier does reasonably well with a classification accuracy of 84.45% on test data. Next, features extracted from both the magnitude and phase signals are concatenated to form a single vector of size 1×375 for each

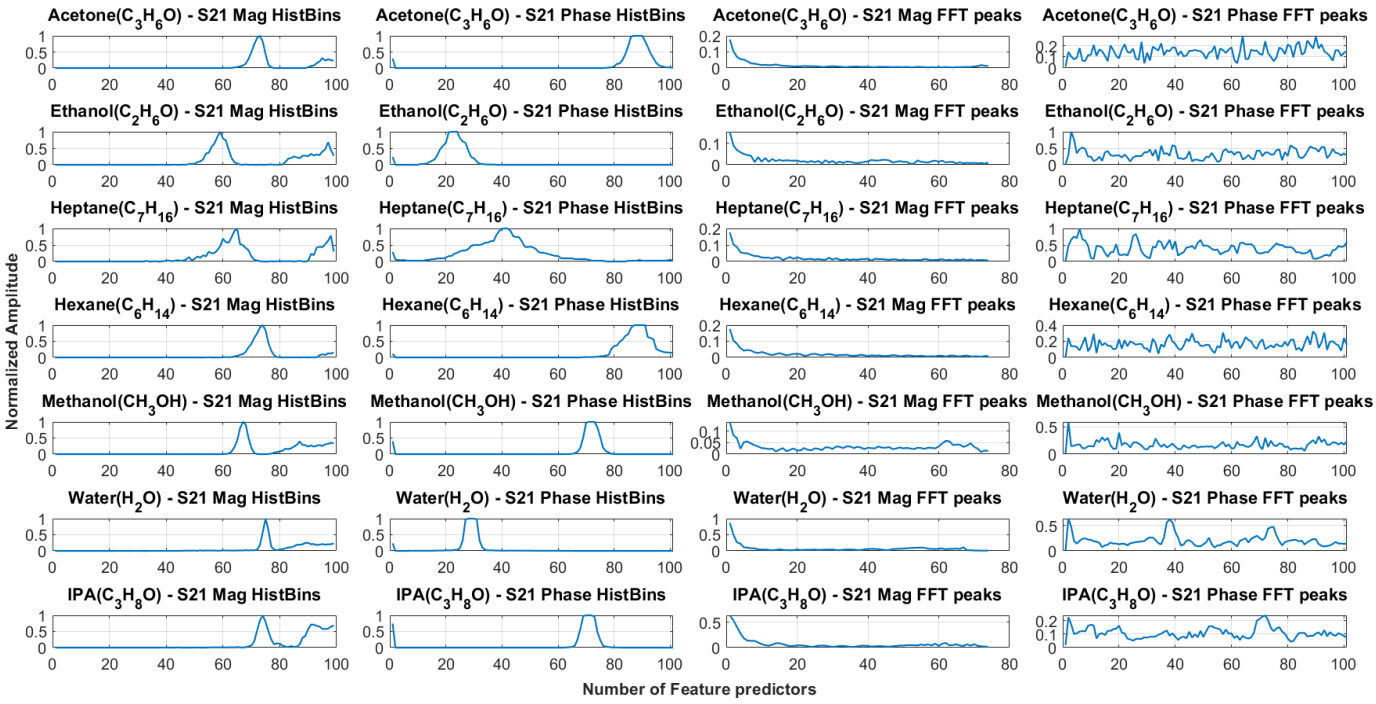

Fig. 8. Feature predictor plot of each liquid used for testing. They show Histogram and FFT peaks extracted from both S21 CW time magnitude and phase signals. These are ultimately concatenated to form a row vector that is given to classifier as a feature predictor of a particular liquid class.

pressures shown in the property TABLE II. It is challenging to give an accurate estimate of evaporation time as the exact droplet size cannot be controlled when performing the dip test. To get an indirect control over the droplet size, the linear motor stage's velocity is set to 10 mm/s for each test. The SMF optical probe was lifted far from the liquid surface to avoid the effect of surface level humidity on evaporation. The distance from droplet to liquid surface was controlled differently for each liquid because the vapor pressure and density of each liquid chemical is unique. In the data acquisition process, the time transient responses and the start time are not identical because of the delays between measurements. Moreover, the start times

liquid sample as shown in Fig. 8. The same 53 measurements were used for training the classifiers with 5-fold cross validation but with features extracted from phase signals. Another set of 27 measurements were acquired as separate hold-out test set for validation after training the classifiers. The hold-out test set was data measured during another experiment which will be used to validate the classifiers' performance. From the training data, a predictor matrix (M_1) of size 374×375 was obtained after feature extraction. From separate hold-out test data, a predictor matrix (M_2) of size 186×375 was obtained after feature extraction, which is nothing, but the features obtained from a separate set of evaporation measurements taken

at different time. The matrix M_1 was split into train matrix of size 187×375 and hold-out test matrix of size 187×375 for K-fold = 2, whose classification results are shown in TABLE III. The matrix M_1 was split into train matrix of size 250×375 and hold-out test matrix of size 124×375 for K-fold = 3, whose classification results are shown in TABLE IV.

From TABLE III and TABLE IV, it can be observed that SVM grants us the highest accuracy greater than 99%. The corresponding confusion matrix for these classifiers is shown in Fig. 8. The confusion matrix gives us information about the number of correctly predicted classes versus the actual classes. When comparing the confusion matrices from Fig. 7 and Fig. 8, it can be observed that the classifiers trained with features extracted from both magnitude and phase signals perform much better than the classifier trained with only features extracted from magnitude signals. The features from magnitude signals provide information regarding only the power variation during the droplet evaporation. However, features from magnitude and phase signals provide both power and length variation information of the droplet evaporation which results in a 15% accuracy improvement. These plots show that the SVM classifier has performed very well in classifying the liquids and

TABLE III
CLASSIFIER TRAINING AND TEST RESULTS FOR 2-FOLD DATA SPLIT

K-FOLD = 2 classifiers	TRAINING ACCURACY (M_1)	TEST ACCURACY (M_1)	TEST ACCURACY on hold-out dataset (M_2)	TOTAL MISCLASSIFICATION COST	TRAINING TIME (seconds)
Decision Tree	94.3%	94.12%	93.01%	11	1.1177
SVM	**99.5%**	**99.35%**	**99.04%**	**1**	**1.6261**
KNN	96.7%	95.2%	95.01%	9	0.7256

The classifiers are trained with 5-fold cross validation in MATLAB's classification learner application on a training dataset of size 187×375, whose accuracy is given in column 2. The classifiers were validated on a test dataset of 187×375, whose accuracy is given in column 3. The classifier was validated on a separate hold-out test dataset of 186×375, whose accuracy is given in column 4. The last two columns give insight into misclassification cost and training time of each classifier.

TABLE IV
CLASSIFIER TRAINING AND TEST RESULTS FOR 3-FOLD DATA SPLIT

K-FOLD = 3 classifiers	TRAINING ACCURACY (M_1)	TEST ACCURACY (M_1)	TEST ACCURACY on hold-out dataset (M_2)	TOTAL MISCLASSIFICATION COST	TRAINING TIME (seconds)
Decision Tree	95.01%	94.15%	94.03%	9	1.1416
SVM	**99.8%**	**99.6%**	**99.56%**	**1**	**1.6691**
KNN	97.6%	95.6%	96.55%	5	0.8283

The classifiers are trained with 5-fold cross validation in MATLAB's classification learner application on a training dataset of size 187×375, whose accuracy is given in column 2. The classifiers were validated on a test dataset of 187×375, whose accuracy is given in column 3. The classifier was validated on a separate hold-out test dataset of 186×375, whose accuracy is given in column 4. The last two columns give insight into misclassification cost and training time of each classifier.

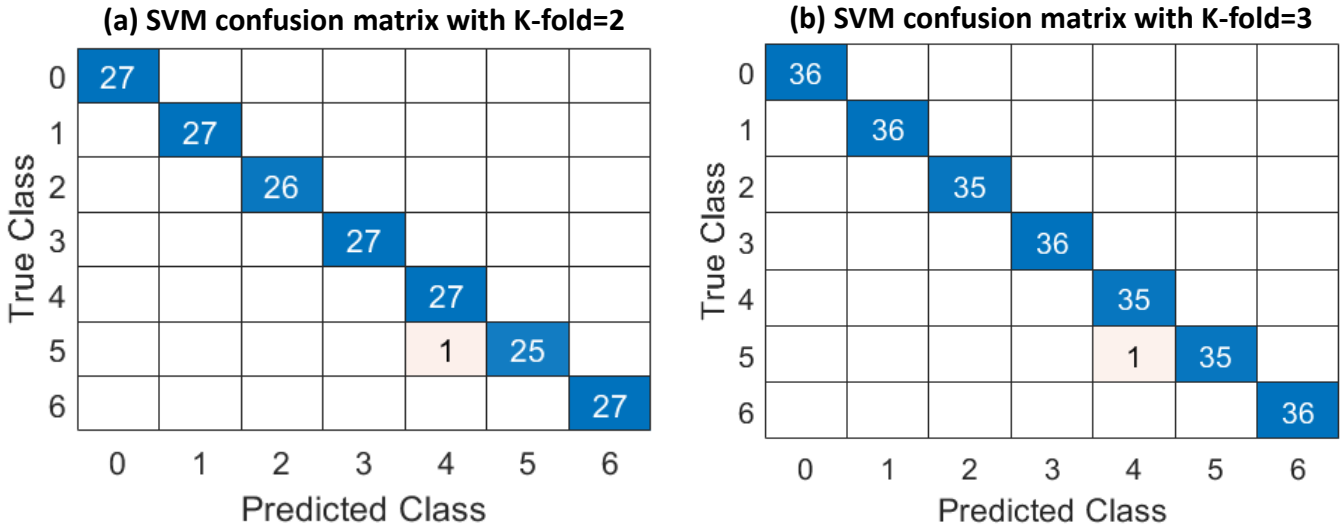

Fig. 9. Confusion matrices to summarize the prediction or classification results on our liquid identification problem. The number of correct and incorrect predictions given for each liquid class for the SVM classifier. (a) SVM with K-fold=2 and (b) SVM with K-fold=3.

are adequate in terms of performance metrics since the dataset is well balanced, i.e., the data used for testing and training have equal number of samples for all the classes. Only one measurement of methanol was misclassified as per Fig. 8, which is attributed to imperfect conditions and measurement uncertainty. Thus, the claim that microwave photonics-based time transient measurements of liquid evaporation phenomenon can be used to classify those liquids by means of traditional machine learning methods is substantiated. Improvement in the measurement selectivity can be done by coating the SMF optical probe tip with targeted chemicals of hydrophobic and hydrophilic nature. It should be possible to record considerably more information in the S21 signals due to the liquid's reaction with coated substance. The use of an array of sensors with different surface coatings allows for a more robust and accurate identification of the liquids by accounting for variations in the evaporation rate and sensing properties of the different liquids on different surfaces.

V. CONCLUSION

In this article, an SMF optical probe with cleaved end face is proposed to monitor the evaporation phenomena of different liquids based on the EFPI formation. A novel approach of training machine learning classifiers with intensity and duration variations of recorded evaporation signals to classify the liquids is successfully presented in this research. A MWP system is used to monitor the evaporation phenomena of liquids as S21 CW time magnitude (intensity) and phase (duration) signals. Features extracted from these S21 CW time signals are concatenated, and machine learning classifiers are trained to identify seven different liquids. The classifier can deliver accuracy above 99% after adequate training. Due to the great sensitivity of EFPIs combined with the MWP measurement approach, we can measure time domain signals with high selectivity, high SNR, high resolution, and fast response. The new measurement approach can be used to research certain pure science phenomena related to the behavior of chemicals and liquids. By assessing alterations in properties like refractive index or vapor pressure during evaporation, valuable insights into a liquid's composition and behavior can be gained. This deepens our understanding in areas such as chemical analysis, health and safety, quality control, chemical research, and biotechnology. Future research will study MWPs extremely selective sensing capabilities, which can shed light on the quantum jump and fluctuations that occur during liquid evaporation. The experimental setup can also be improved by using an array of fiber optic cables with different coatings at the fiber end face to obtain richer features pertaining to liquid droplet evaporation. The detection of boundary between binary liquid mixtures is also being studied with MWP sensing system. In addition, the MWP-based time transient measurement for the evaporation process combined with data analytics like machine learning opens a new subject of exploration in the sensing field.

REFERENCES

[1] Erbil, H. Yildirim. "Evaporation of pure liquid sessile and spherical suspended drops: A review." Advances in colloid and interface science 170.1-2 (2012): 67-86.

[2] Matlosz, R. L., S. Leipziger, and T. P. Torda. "Investigation of liquid drop evaporation in a high temperature and high-pressure environment." International Journal of Heat and Mass Transfer 15.4 (1972): 831-852.

[3] Xiong, T. Y., and M. C. Yuen. "Evaporation of a liquid droplet on a hot plate." International journal of heat and mass transfer 34.7 (1991): 1881-1894.

[4] Abu-Zaid, M. "An experimental study of the evaporation characteristics of emulsified liquid droplets." Heat and mass transfer 40.9 (2004): 737-741.

[5] Zeid, W. Bou, J. Vicente, and David Brutin. "Influence of evaporation rate on cracks' formation of a drying drop of whole blood." Colloids and Surfaces A: Physicochemical and Engineering Aspects 432 (2013): 139-146.

[6] Al Qubeissi, Mansour, et al. "Heating and Evaporation of Droplets of Multicomponent and Blended Fuels: A Review of Recent Modeling Approaches." Energy \& Fuels 35.22 (2021): 18220-18256.

[7] Teske, Milton E., Clarence G. Hermansky, and Christopher M. Riley. "Evaporation rates of agricultural spray material at low relative wind speeds." Atomization and Sprays 8.4 (1998).

[8] Herbst, M., et al. "Simultaneous measurements of transpiration, soil evaporation and total evaporation in a maize field in northern Germany." Journal of Experimental Botany 47.12 (1996): 1957-1962.

[9] Fujiyasu, Yoshimasa, and Martin Fahey. "Experimental study of evaporation from saline tailings." Journal of geotechnical and geoenvironmental engineering 126.1 (2000): 18-27.

[10] Fukatani, Yuki, et al. "Effect of ambient temperature and relative humidity on interfacial temperature during early stages of drop evaporation." Physical Review E 93.4 (2016): 043103.

[11] Tang, I. N., and H. R. Munkelwitz. "Determination of vapor pressure from droplet evaporation kinetics." Journal of colloid and interface science 141.1 (1991): 109-118.

[12] O'Hare, K. D., and P. L. Spedding. "Evaporation of a binary liquid mixture." The Chemical Engineering Journal 48.1 (1992): 1-9.

[13] Kamai, Tamir, Noam Weisbrod, and Maria Inés Dragila. "Impact of ambient temperature on evaporation from surface-exposed fractures." Water resources research 45.2 (2009).

[14] Qu, Jie, et al. "Experimental study of evaporation and crystallization of brine droplets under different temperatures and humidity levels." International Communications in Heat and Mass Transfer 110 (2020): 104427.

[15] Pearlmutter, David, E. L. Krüger, and P. Berliner. "The role of evaporation in the energy balance of an open-air scaled urban surface." International Journal of Climatology: A Journal of the Royal Meteorological Society 29.6 (2009): 911-920.

[16] Gunda, Naga Siva Kumar, Saumyadeb Dasgupta, and Sushanta K. Mitra. "DipTest: A litmus test for E. coli detection in water." PLoS One 12.9 (2017): e0183234.

[17] Zhang, Weixin, et al. "Water-evaporation-induced self-assembly of α-MnO2 hierarchical hollow nanospheres and their applications in ammonia gas sensing." Sensors and Actuators B: Chemical 162.1 (2012): 292-299.

[18] Zhou, Qiong, et al. "A Chinese liquor classification method based on liquid evaporation with one unmodulated metal oxide gas sensor." Sensors and Actuators B: Chemical 160.1 (2011): 483-489.

[19] Arcamone, Julien, et al. "Evaporation of femtoliter sessile droplets monitored with nanomechanical mass sensors." The Journal of Physical Chemistry B 111.45 (2007): 13020-13027.

[20] K. Park, N. Kim, D. T. Morisette, N. R. Aluru and R. Bashir, "Resonant MEMS Mass Sensors for Measurement of Microdroplet Evaporation," in Journal of Microelectromechanical Systems, vol. 21, no. 3, pp. 702-711, June 2012, doi: 10.1109/JMEMS.2012.2189359.

[21] Jung, Insup, et al. "A dip-stick type biosensor using bioluminescent bacteria encapsulated in color-coded alginate microbeads for detection of water toxicity." Analyst 139.18 (2014): 4696-4701.

[22] Belford, Earel M., et al. "Evaluation of a new chemical dip strip for detecting ketonemia in the emergency setting." The American journal of emergency medicine 5.5 (1987): 393-394.

[23] Xie, Weiguo, et al. "Fibre optic chemical sensor systems for internal concrete condition monitoring." Second European Workshop on Optical Fibre Sensors. Vol. 5502. SPIE, 2004.

[24] Wassana Naku, Chen Zhu, Anand K. Nambisan, Rex E. Gerald, and Jie Huang, "Machine learning identifies liquids employing a simple fiber-optic tip sensor," Opt. Express 29, 40000-40014 (2021)

[25] Preter, Eyal, et al. "Monitoring and analysis of pendant droplets evaporation using bare and monolayer-coated optical fiber facets." Optical Materials Express 4.5 (2014): 903-915.

[26] Uemura, Suguru, et al. "Picoliter droplet formation on thin optical fiber tips." Langmuir 22.24 (2006): 10272-10276.

[27] Ramakrishnan, Manjusha, et al. "Overview of fiber optic sensor technologies for strain/temperature sensing applications in composite materials." Sensors 16.1 (2016): 99.

[28] Roman, Muhammad, et al. "A spatially distributed fiber-optic temperature sensor for applications in the steel industry." Sensors 20.14 (2020): 3900.

[29] Berthold, J., W. Ghering, and D. Varshneya. "Design and characterization of a high temperature fiber-optic pressure transducer." Journal of lightwave technology 5.7 (1987): 870-876.

[30] Liu, Guigen, et al. "Optical fiber vector flow sensor based on a silicon Fabry–Perot interferometer array." Optics letters 41.20 (2016): 4629-4632.

[31] Lei, Ying-Jun, et al. "Optical Accelerometers for Detecting Low-Frequency Micro-Vibrations." Applied Sciences 12.8 (2022): 3994.

[32] Zhu, Yizheng, and Anbo Wang. "Miniature fiber-optic pressure sensor." IEEE Photonics Technology Letters 17.2 (2005): 447-449.

[33] Jorgenson, Ralph C., and Sinclair S. Yee. "A fiber-optic chemical sensor based on surface plasmon resonance." Sensors and Actuators B: Chemical 12.3 (1993): 213-220.

[34] Warren-Smith, Stephen C., and Tanya M. Monro. "Exposed core microstructured optical fiber Bragg gratings: refractive index sensing." Optics express 22.2 (2014): 1480-1489.

[35] Lu, Xin, Peter James Thomas, and Jon Oddvar Hellevang. "A review of methods for fibre-optic distributed chemical sensing." Sensors 19.13 (2019): 2876.

[36] Zeakes, Jason S., et al. "Modified extrinsic Fabry-Perot interferometric hydrogen gas sensor." Proceedings of LEOS'94. Vol. 2. IEEE, 1994.

[37] Bhatia, Vikram, et al. "Recent developments in optical-fiber-based extrinsic Fabry-Perot interferometric strain sensing technology." Smart Materials and Structures 4.4 (1995): 246.

[38] McGuinness, Fintan, et al. "Fabrication and Qualitative Analysis of an Optical Fibre EFPI-Based Temperature Sensor." Sensors 21.13 (2021): 4445.

[39] Yu, Qingxu, and Xinlei Zhou. "Pressure sensor based on the fiber-optic extrinsic Fabry-Perot interferometer." Photonic Sensors 1.1 (2011): 72-83.

[40] C. Zhu, Y. Zhuang, B. Zhang, R. Muhammad, P. P. Wang and J. Huang, "A Miniaturized Optical Fiber Tip High-Temperature Sensor Based on Concave-Shaped Fabry–Perot Cavity," in IEEE Photonics Technology Letters, vol. 31, no. 1, pp. 35-38, 1 Jan.1, 2019, doi: 10.1109/LPT.2018.2881721.

[41] K. Bremer, E. Lewis, G. Leen, B. Moss, S. Lochmann and I. A. R. Mueller, "Feedback Stabilized Interrogation Technique for EFPI/FBG Hybrid Fiber-Optic Pressure and Temperature Sensors," in IEEE Sensors Journal, vol. 12, no. 1, pp. 133-138, Jan. 2012, doi: 10.1109/JSEN.2011.2140104.

[42] J. E. Alfonso, L. G. Cárdenas, C. A. Triana and M. V. Durán, "Design of an optical sensing interrogator using an edge filter scheme," 2013 SBMO/IEEE MTT-S International Microwave \& Optoelectronics Conference (IMOC), 2013, pp. 1-5, doi: 10.1109/IMOC.2013.6646509.

[43] Yu, Bing, et al. "Tunable-optical-filter-based white-light interferometry for sensing." Optics letters 30.12 (2005): 1452-1454.

[44] Yao, Jianping. "Microwave photonics for high-resolution and high-speed interrogation of fiber Bragg grating sensors." Fiber and Integrated Optics 34.4 (2015): 204-216.

[45] J. Hervás et al., "Microwave Photonics for Optical Sensors," in IEEE Journal of Selected Topics in Quantum Electronics, vol. 23, no. 2, pp. 327-339, March-April 2017, Art no. 5602013, doi: 10.1109/JSTQE.2017.2651117.

[46] H. Deng, W. Zhang and J. Yao, "High-Speed and High-Resolution Interrogation of a Silicon Photonic Microdisk Sensor Based on Microwave Photonic Filtering," in Journal of Lightwave Technology, vol. 36, no. 19, pp. 4243-4249, Oct.1, 2018, doi: 10.1109/JLT.2018.2843724.

[47] Cheng, Baokai, et al. "Microwave photonic distributed sensing in harsh environment." Micro-and Nanotechnology Sensors, Systems, and Applications VIII. Vol. 9836. SPIE, 2016.

[48] Zhu, Chen, et al. "Distributed fiber optic sensing with enhanced sensitivity based on microwave-photonic Vernier effect." Optics Letters 47.11 (2022): 2810-2813.

[49] Kim, Han-Su, et al. "Unoxidized porous Si as an isolation material for mixed-signal integrated circuit applications." Journal of applied physics 93.7 (2003): 4226-4231.

[50] G. Gennarelli, S. Romeo, M. R. Scarfì and F. Soldovieri, "A Microwave Resonant Sensor for Concentration Measurements of Liquid Solutions," in IEEE Sensors Journal, vol. 13, no. 5, pp. 1857-1864, May 2013, doi: 10.1109/JSEN.2013.2244035.

[51] Buford, Randall Jean, Eric C. Green, and Melanie J. McClung. "A microwave frequency sensor for non-invasive blood-glucose measurement." 2008 IEEE Sensors Applications Symposium. IEEE, 2008.

[52] V. Ricchiuti, "Power bus signal integrity improvement and EMI mitigation on multilayer high-speed digital PCBs with embedded capacitance," in IEEE Transactions on Mobile Computing, vol. 2, no. 4, pp. 314-321, Oct.-Dec. 2003, doi: 10.1109/TMC.2003.1255646.

[53] J. Murdock, E. Ben-Dor, F. Gutierrez and T. S. Rappaport, "Challenges and approaches to on-chip millimeter wave antenna pattern measurements," 2011 IEEE MTT-S International Microwave Symposium, 2011, pp. 1-4, doi: 10.1109/MWSYM.2011.5972965.

[54] Wei, W. Yu, and Ian M. White. "A simple filter-based approach to surface enhanced Raman spectroscopy for trace chemical detection." Analyst 137.5 (2012): 1168-1173.

[55] Kirsch, Jeffrey, et al. "Biosensor technology: recent advances in threat agent detection and medicine." Chemical Society Reviews 42.22 (2013): 8733-8768.

[56] Sigman, Michael E., et al. "Ignitable liquid classification and identification using the summed-ion mass spectrum." Instrumentation Science and Technology 36.4 (2008): 375-393.

[57] Cong, Jun, et al. "Fiber optic Bragg grating sensor based on hydrogels for measuring salinity." Sensors and Actuators B: Chemical 87.3 (2002): 487-490.

[58] Yang, Lin, et al. "Detection of kerosene adulteration in automobile fuel by a low-loss surface plasmon resonance (SPR) chemical sensor." Analytical Methods (2022).

[59] Yaqoob, Usman, and Mohammad I. Younis. "Chemical gas sensors: Recent developments, challenges, and the potential of machine learning—A review." Sensors 21.8 (2021): 2877.

[60] Cho, Soo-Yeon, et al. "Finding hidden signals in chemical sensors using deep learning." Analytical chemistry 92.9 (2020): 6529-6537.

[61] Jiao, Zeren, et al. "Machine learning and deep learning in chemical health and safety: a systematic review of techniques and applications." ACS Chemical Health & Safety 27.6 (2020): 316-334.

[62] Zdravevski, Eftim, et al. "Robust histogram-based feature engineering of time series data." 2015 Federated Conference on Computer Science and Information Systems (FedCSIS). IEEE, 2015.

[63] Leandro, Daniel, et al. "Real-time FFT analysis for interferometric sensors multiplexing." Journal of Lightwave Technology 33.2 (2015): 354-360.

[64] Bhatia, Jyoti, et al. "Object classification technique for mmWave FMCW radars using range-FFT features." 2021 International Conference on COMmunication Systems & NETworkS (COMSNETS). IEEE, 2021.

[65] Polat, Kemal, and Salih Güneş. "Classification of epileptiform EEG using a hybrid system based on decision tree classifier and fast Fourier transform." Applied Mathematics and Computation 187.2 (2007): 1017-1026.

[66] Huang, Jie, et al. "Optical carrier-based microwave interferometers for sensing application." Fiber Optic Sensors and Applications XI. Vol. 9098. SPIE, 2014.

[67] Übeyli, Elif Derya. "ECG beats classification using multiclass support vector machines with error correcting output codes." Digital Signal Processing 17.3 (2007): 675-684.

[68] Naku, Wassana, et al. "Identification of Volatile Organic Liquids by Combining an Array of Fiber-Optic Sensors and Machine Learning." ACS Omega (2023).

[69] Tankovsky, N., and N. Zografov. "Evaporation-rate dynamics of a hemispherical, pendant liquid droplet, influenced by resonant oscillations." Colloid and Interface Science Communications 12 (2016): 5-8.

[70] Perakis, Fivos, et al. "Vibrational spectroscopy and dynamics of water." Chemical reviews 116.13 (2016): 7590-7607.